Effect of absorption on terahertz surface plasmon polaritons propagating along periodically corrugated metal wires

Linfang Shen
Department of Information Science and Electronic Engineering, Electromagnetic Academy, Zhejiang University, Zhejiang Province, Hangzhou 310027, People's Republic of China

Xudong Chen,* Yu Zhong, and Krishna Agarwal
Department of Electrical and Computer Engineering, National University of Singapore, Singapore 117576, Singapore
(Received 3 August 2007; published 11 February 2008)

In this paper, a rigorous method for analyzing surface plasmon polaritons (SPPs) on a periodically corrugated metal wire has been formulated, based on a modal expansion of electromagnetic fields. Compared with the previous method, our method takes into account the finite conductivity of the wire as well as higher-order modes within the wire grooves in the expansion, thus is able to accurately calculate the loss of these spoof SPPs propagating along the wire. In the terahertz frequency range, the properties of the loss of spoof SPPs on corrugated Al wires are analyzed. The loss of the spoof SPPs grows significantly with the increase of field confinement, and it is often considerably large when the frequency is close to the asymptotic frequency. The effect of absorption on the energy concentration and superfocusing of terahertz radiation is also analyzed, and found to be tolerably small, except very close to the asymptotic frequency.

DOI: 10.1103/PhysRevB.77.075408 PACS number(s): 73.20.Mf, 42.25.Bs, 42.79.Gn, 78.68.+m

Surface plasmon polaritons (SPPs) at metal-dielectric interfaces have recently attracted much attention for their relevance in subwavelength optics and nanophotonics.[1–4] While most studies of SPPs focus on the visible and infrared frequency ranges, there has been increasing interest in the study of SPPs in the terahertz regime.[5–7] At terahertz frequencies, however, metals resemble a perfect conductor as their plasma frequencies are often in the utraviolet part of the spectrum, leading to SPPs highly delocalized on both flat and cylindrical surfaces. As a consequence, SPPs suffer serious radiation loss (due to bends and nearby objects) and cross-talk (between two wires). To enable high field confinement at lower frequencies, an idea of engineering surface plasmon at any frequency was proposed.[8,9] That is, by cutting holes or grooves in flat metal surfaces to increase the penetration of electromagnetic (EM) fields into the metal, the frequency of existing surface plasmons can be tailored at will. The existence of such geometry-controlled SPPs, named, *spoof* SPPs, has recently been verified experimentally in the microwave regime.[10] More recently, it has been reported that spoof SPPs at terahertz frequencies can also be sustained on periodically corrugated metal wires.[11,12] The energy concentration and superfocusing of terahertz radiation in a corrugated wire or cone were also demonstrated,[11] which have promising applications in terahertz imaging and spectrocopy. In these theoretical studies,[11,12] metals were all approximated by a perfect electric conductor (PEC), so that spoof SPPs are lossless as they propagate along the wire. However, as the dielectric effect of metals at terahertz frequencies is enhanced in cylindrically shaped geometry,[13] the loss of these spoof SPPs could not be neglected due to the absorption in metal, especially when the fields associated with the SPPs are highly confined to the surface of the wire. For the development of plasmonic devices based on corrugated wire structures, a detailed knowledge of the characteristic of spoof SPPs is essential. In this paper, we will study the loss properties of spoof SPPs on aluminum (Al) wires corrugated periodically with grooves. For this purpose, a rigorous method for analyzing these spoof SPPs is formulated based on a modal expansion of EM fields.[14] The finite conductivity of the wire as well as higher-order modes within the wire grooves are taken into account in this formulation.

Consider a metal wire of radius R in which an array of radial grooves of depth $h=R-r$, width a, and lattice constant d is milled, as illustrated in the inset of Fig. 1(a). We are interested in TM-polarized surface waves with azimuthal (ϕ) symmetry propagating in the z direction along the wire. The fields of these waves have the form of $\mathbf{H}=\hat{\phi}H_\phi$ and $\mathbf{E}=\hat{\rho}E_\rho+\hat{z}E_z$. In Refs. 11 and 12, this type of surface waves is analyzed by the modal expansion method, but the metal wire is treated as PEC and only the lowest-order eigenmode inside the wire grooves is counted. The modal expansion method used in this paper takes into account the finite conductivity of the wire as well as higher-order modes within the wire grooves. In region I ($\rho>R$), the azimuthal component of the magnetic field ($\mathbf{H}$), which is nonradiative and vanishes as $\rho\to\infty$, can be written as

$$H_\phi^{\mathrm{I}}(\rho,z)=\sum_n A_n^{(1)}K_1(q_n^{(1)}\rho)e^{i\beta_n z}, \tag{1}$$

where $A_n^{(1)}$ are constants, $\beta_n=\beta+2\pi n/d$ [here, the propagation constant of the surface wave lies in the first Brillouin zone, i.e., $|\mathrm{Re}(\beta)|\leqslant\pi/d$, where $\mathrm{Re}(\cdot)$ denotes real part operator], and $q_n^{(1)}=\sqrt{(\beta_n)^2-k_0^2}$, with k_0 being the wave number in free space; K_1 is the first-order modified Neumann function. In region III ($0\leqslant\rho<r$), H_ϕ is similarly written as

$$H_\phi^{\mathrm{III}}(\rho,z)=\sum_n A_n^{(3)}I_1(q_n^{(3)}\rho)e^{i\beta_n z}, \tag{2}$$

where $A_n^{(3)}$ are constants, $q_n^{(3)}=\sqrt{(\beta_n)^2-\varepsilon_m k_0^2}$, and ε_m is the relative permittivity of the metal; I_1 is the first-order modi-

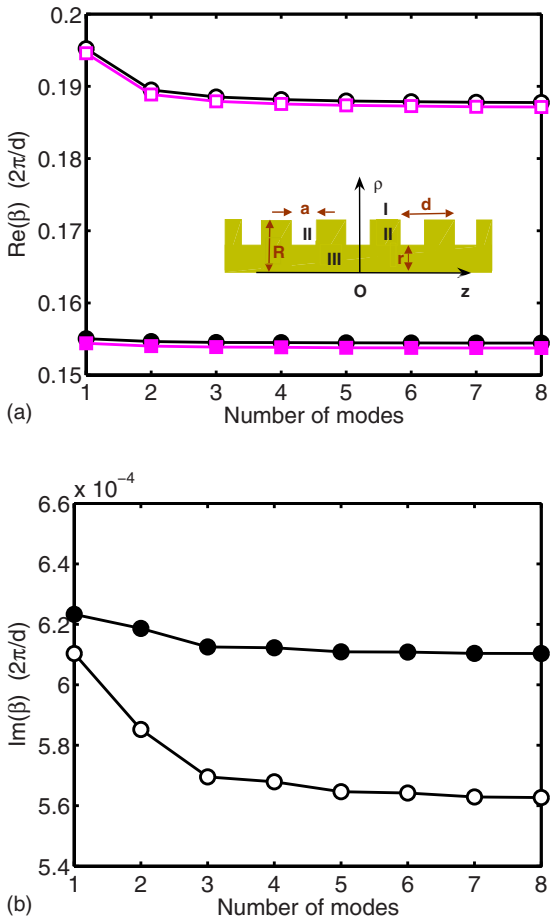

FIG. 1. (Color online) Convergence of the (a) real and (b) imaginary parts of the propagation constant β calculated from Eq. (17) for $d=50$ μm, $R=100$ μm, and $f=0.8$ THz. The corresponding results obtained within the PEC approximation are included as squares for comparison. The wire geometry is shown in the inset. Solid marks correspond to the groove case of $a=0.2d$ and $h=d$, and open marks correspond to the case of $a=0.6d$ and $h=0.9d$.

fied Bessel function. On the other hand, since the metal thickness between the grooves $(d-a)$ is much larger than the skin depth for terahertz frequencies, the fields in the part of the unit cell in region II $(r \leqslant \rho \leqslant R)$ can be treated as a superposition of eigenmodes with azimuthal symmetry in an isolated groove waveguide. Thus, H_ϕ in this part of the unit cell is expressed as

$$H_\phi^{\mathrm{II}}(\rho,z) = \sum_m [A_m^{(2)} H_1^{(1)}(g_m\rho) + B_m^{(2)} H_1^{(2)}(g_m\rho)]\psi_m(z), \quad (3)$$

where $A_m^{(2)}$ and $B_m^{(2)}$ are constants, $H_1^{(1)}$ and $H_1^{(2)}$ are the first- and second-kind Hankel functions, respectively, and the modal field profiles ψ_m are given by

$$\psi_m(z) = \begin{cases} f(p_m a/2)e^{-\gamma_m(z-a/2)}, & z > a/2 \\ f(p_m z), & |z| \leqslant a/2 \\ f(-p_m a/2)e^{\gamma_m(z+a/2)}, & z < -a/2, \end{cases}$$

where $p_m=\sqrt{k_0^2-g_m^2}$, $\gamma_m=\sqrt{g_m^2-\varepsilon_m k_0^2}$, and the function $f(x)=\cos(x)$ for symmetric modes with even m $(m=0,2,\ldots)$, or $f(x)=\sin(x)$ for asymmetric modes with odd m $(m=1,3,\ldots)$. Here, g_m and p_m are governed by the dispersion relation: $\tan(p_m a/2)=\gamma_m/(\varepsilon_m p_m)$ for even m, or $\tan(p_m a/2-\pi/2)=\gamma_m/(\varepsilon_m p_m)$ for odd m. Note that these eigenmodes with azimuthal symmetry propagate like a cylindrical wave in the propagation plane orthogonal to the z direction, and each of them can be decomposed into a number of ordinary eigenmodes of the same propagation constant and field profile, which propagate like a plane wave in that propagation plane. In mathematics, this corresponds to the integral representation for Hankel functions. From the properties of ordinary modes in a parallel-plate waveguide, it is clear that the functions ψ_m also satisfy the orthogonality[15]

$$\frac{1}{a}\int_{-d/2}^{d/2} \frac{1}{\varepsilon(z)}\psi_m\psi_n dz \approx \frac{1}{a}\int_{-\infty}^{\infty} \frac{1}{\varepsilon(z)}\psi_m\psi_n dz = N_m\delta_{mn}, \quad (4)$$

where $\varepsilon(z)=1$ for $|z|\leqslant a/2$ and $\varepsilon(z)=\varepsilon_m$ elsewhere, and N_m is a coefficient depending on the value of m.

The nonzero components (E_ρ and E_z) of the electric field ($\mathbf{E}$) can be obtained straightforwardly from H_ϕ. The parallel components of $\mathbf{E}$ and $\mathbf{H}$ must be continuous at the interface between regions I and II, and the one between regions II and III. In a way similar to that described in Ref. 14, from the continuity of H_ϕ and E_z at the interface $\rho=R$, we obtain

$$\sum_n A_n^{(1)} K_1(q_n^{(1)}R) S_{mn}^{+} = [A_m^{(2)} H_1^{(1)}(g_m R) + B_m^{(2)} H_1^{(2)}(g_m R)]N_m, \quad (5)$$

where the orthogonality property for functions $\psi_m(z)$ has been used, and

$$-A_n^{(1)} q_n^{(1)} K_0(q_n^{(1)}R) = \frac{a}{d}\sum_m g_m [A_m^{(2)} H_0^{(1)}(g_m R) + B_m^{(2)} H_0^{(2)}(g_m R)]S_{mn}^{-}, \quad (6)$$

where the orthogonality property for $\exp(i\beta_n z)$, i.e., $(1/d)\int_{-d/2}^{d/2}\exp(i\beta_n z)\exp(-i\beta_{n'}z)dz=\delta_{nn'}$, has been used. The coefficients N_m are defined in Eq. (4), and $S_{mn}^{\pm}$ are defined as

$$S_{mn}^{\pm} = \frac{1}{a}\int_{-d/2}^{d/2} \frac{1}{\varepsilon(z)}\psi_m(z)\exp(\pm i\beta_n z)dz.$$

Substitution of Eq. (6) into Eq. (5) yields

$$A_m^{(2)} H_1^{(1)}(g_m R) + B_m^{(2)} H_1^{(2)}(g_m R) = -\frac{k_0}{q_0^{(1)}}\sum_{m'} U_{mm'}[A_{m'}^{(2)} H_0^{(1)}(g_{m'}R) + B_{m'}^{(2)} H_0^{(2)}(g_{m'}R)], \quad (7)$$

where $U_{mm'}$ are given by

$$U_{mm'} = \frac{a}{dN_m}\frac{g_{m'}}{k_0}\sum_n \frac{q_0^{(1)} K_1(q_n^{(1)}R)}{q_n^{(1)} K_0(q_n^{(1)}R)} S_{mn}^{+} S_{m'n}^{-}.$$

Similarly, from the continuity of H_ϕ and E_z at the interface $\rho=r$, we can obtain

$$A_m^{(2)}H_1^{(1)}(g_m r) + B_m^{(2)}H_1^{(2)}(g_m r) = -\sqrt{-\varepsilon_m}\sum_{m'} V_{mm'}[A_{m'}^{(2)}H_0^{(1)}(g_{m'} r) + B_{m'}^{(2)}H_0^{(2)}(g_{m'} r)], \tag{8}$$

where $V_{mm'}$ are given by

$$V_{mm'} = \frac{a}{dN_m}\frac{g_{m'}}{k_0}\sum_n \frac{I_1(q_n^{(3)} r)}{I_0(q_n^{(3)} r)} S_{mn}^{+} S_{m'n}^{-}.$$

Note that $q_n^{(3)} \approx \sqrt{-\varepsilon_m} k_0$ since $|\varepsilon_m|$ is often very large for terahertz frequencies. The usual approach for obtaining the dispersion equation is to substitute Eq. (8) into Eq. (7), which eliminates coefficients $B_m^{(2)}$ and yields a matrix equation $Q[A^{(2)}] = (q_0^{(1)}/k_0)[A^{(2)}]$, where the vector $[A^{(2)}]$ has a length equal to the number of the modes included in Eq. (3). Thus, it follows that the dispersion equation is $\det\{Q - (q_0^{(1)}/k_0)I\} = 0$, where I is a unit matrix, and $\det\{\cdot\}$ denotes the determinant. However, this dispersion equation for spoof SPPs is difficult to solve numerically, because the matrix Q is severely ill-conditioned in the case of our interest. The reason is that since modes with high orders ($m \geqslant 1$) in the groove waveguide are evanescent, the parameters g_m have a large (positive) imaginary part, i.e., $\mathrm{Im}(g_m) \approx \sqrt{(m\pi/a)^2 - k_0^2} \approx m\pi/a$ [here $\mathrm{Im}(\cdot)$ denotes imaginary part operator], thus the values of the second-kind Hankel functions in Eqs. (7) and (8) may become intolerably large in the computation.

To deal with this problem, we first let $\bar{A}_m = A_m^{(2)} H_0^{(1)}(\bar{\rho}_{2m})\alpha_m$ and $\bar{B}_m = B_m^{(2)} H_0^{(2)}(\bar{\rho}_{2m})\alpha_m^{-1}$, where $\alpha_m = [H_0^{(1)}(\bar{\rho}_{1m})/H_0^{(1)}(\bar{\rho}_{2m})]^{1/4}[H_0^{(2)}(\bar{\rho}_{2m})/H_0^{(2)}(\bar{\rho}_{1m})]^{1/4}$, $\bar{\rho}_{1m} = g_m R$, and $\bar{\rho}_{2m} = g_m r$, and rewrite Eqs. (7) and (8), respectively, as

$$[\zeta_m^{+}(\bar{A}_m\alpha_m + \bar{B}_m\alpha_m^{-1}) + \zeta_m^{-}(\bar{A}_m\alpha_m - \bar{B}_m\alpha_m^{-1})]\kappa_m = -\frac{k_0}{q_0^{(1)}}\sum_{m'} U_{mm'}\kappa_{m'}(\bar{A}_{m'}\alpha_{m'} + \bar{B}_{m'}\alpha_{m'}^{-1}), \tag{9}$$

$$\eta_m^{+}(\bar{A}_m\alpha_m^{-1} + \bar{B}_m\alpha_m) + \eta_m^{-}(\bar{A}_m\alpha_m^{-1} - \bar{B}_m\alpha_m) = -\sqrt{-\varepsilon_m}\sum_{m'} V_{mm'}(\bar{A}_{m'}\alpha_{m'}^{-1} + \bar{B}_{m'}\alpha_{m'}), \tag{10}$$

where

$$\kappa_m = [H_0^{(1)}(\bar{\rho}_{1m})/H_0^{(1)}(\bar{\rho}_{2m})]^{1/2}[H_0^{(2)}(\bar{\rho}_{1m})/H_0^{(2)}(\bar{\rho}_{2m})]^{1/2},$$

$$\zeta_m^{\pm} = [H_1^{(1)}(\bar{\rho}_{1m})/H_0^{(1)}(\bar{\rho}_{1m}) \pm H_1^{(2)}(\bar{\rho}_{1m})/H_0^{(2)}(\bar{\rho}_{1m})]/2,$$

$$\eta_m^{\pm} = [H_1^{(1)}(\bar{\rho}_{2m})/H_0^{(1)}(\bar{\rho}_{2m}) \pm H_1^{(2)}(\bar{\rho}_{2m})/H_0^{(2)}(\bar{\rho}_{2m})]/2.$$

Apparently, the quantities κ_m, $\zeta_m^{\pm}$, and $\eta_m^{\pm}$ in Eqs. (9) and (10) are all not very large, but this is not the case for α_m^{-1}. Therefore, we further let $x_m = (\bar{A}_m + \bar{B}_m)(\alpha_m^{-1} + \alpha_m)/2$ and $y_m = (\bar{A}_m - \bar{B}_m)(\alpha_m^{-1} - \alpha_m)/2$, then Eqs. (9) and (10) become

$$[(\zeta_m^{+} - t_m\zeta_m^{-})x_m - (\zeta_m^{+} - t_m^{-1}\zeta_m^{-})y_m]\kappa_m = -\frac{k_0}{q_0^{(1)}}\sum_{m'} U_{mm'}\kappa_{m'}(x_{m'} - y_{m'}), \tag{11}$$

$$(\eta_m^{+} + t_m\eta_m^{-})x_m + (\eta_m^{+} + t_m^{-1}\eta_m^{-})y_m = -\sqrt{-\varepsilon_m}\sum_{m'} V_{mm'}(x_{m'} + y_{m'}), \tag{12}$$

respectively, where $t_m = (\alpha_m^{-1} - \alpha_m)/(\alpha_m^{-1} + \alpha_m)$ are also not large. Equations (11) and (12) can be expressed in a matrix form

$$M_1 X - M_2 Y = -\frac{k_0}{q_0^{(1)}} U(X - Y), \tag{13}$$

$$L_1 X + L_2 Y = -\sqrt{-\varepsilon_m} KVK^{-1}(X + Y), \tag{14}$$

where the vectors X and Y are defined as $X_m = \kappa_m x_m$ and $Y_m = \kappa_m y_m$. The diagonal matrices L_1, L_2, M_1, M_2, and K are defined as follows: $(L_1)_{mm'} = (\eta_m^{+} + t_m\eta_m^{-})\delta_{mm'}$, $(L_2)_{mm'} = (\eta_m^{+} + t_m^{-1}\eta_m^{-})\delta_{mm'}$, $(M_1)_{mm'} = (\zeta_m^{+} - t_m\zeta_m^{-})\delta_{mm'}$, $(M_2)_{mm'} = (\zeta_m^{+} - t_m^{-1}\zeta_m^{-})\delta_{mm'}$, and $K_{mm'} = \kappa_m\delta_{mm'}$. From Eq. (14), we have

$$X + Y \approx -\frac{1}{\sqrt{-\varepsilon_m}} KV^{-1}K^{-1}(L_1 - L_2)X, \tag{15}$$

where we have used the approximation $(KVK^{-1} + L_2/\sqrt{-\varepsilon_m})^{-1} \approx KV^{-1}K^{-1} - (KV^{-1}K^{-1})L_2(KV^{-1}K^{-1})/\sqrt{-\varepsilon_m}$. Note that $|\varepsilon_m|$ is very large for terahertz frequencies and higher-order terms of $1/\sqrt{-\varepsilon_m}$ are dropped off. From Eqs. (13) and (15), we find $QX = (q_0^{(1)}/k_0)X$ with

$$Q = -(M_1 + M_2)^{-1}\left[2U + \frac{1}{\sqrt{-\varepsilon_m}}\left(U + \frac{q_0^{(1)}}{k_0}M_2\right) \times (KV^{-1}K^{-1})(L_1 - L_2)\right]. \tag{16}$$

Thus, we obtain the dispersion relation for spoof SPPs on the corrugated wire as

$$\det\left\{Q - \frac{q_0^{(1)}}{k_0}I\right\} = 0, \tag{17}$$

where I is a unit matrix. Note that $q_0^{(1)} = \sqrt{\beta^2 - k_0^2}$. Equation (17) can be solved numerically via iteration for $q_0^{(1)}$ or β. If an estimate for $q_0^{(1)}$ is given, we can calculate the matrix Q from Eq. (16), and then find the next estimate for $q_0^{(1)}$ through solving for the eigenvalue of the matrix Q from Eq. (17). The iteration proceeds until the estimated $q_0^{(1)}$ converges sufficiently. If the metal is a PEC, i.e., $|\varepsilon_m| \to \infty$, Eq. (16) reduces to $Q = -2(M_1 + M_2)^{-1}U$, and Eq. (17) becomes $\det\{2(M_1 + M_2)^{-1}U + (q_0^{(1)}/k_0)I\} = 0$. Our analysis shows that this dispersion equation can be simplified to Eq. (3) of Ref. 11, if only the lowest-order ($m = 0$) mode of the groove waveguide is included in the field expansion. In the limit $R, r \gg \lambda$ and $\lambda \gg d$, this dispersion equation can be further simplified to $q_0^{(1)} = (a/d)k_0 \tan(k_0 h)$,[9,11] which offers an initial

estimate for $q_0^{(1)}$ in solving Eq. (17). In the PEC case, the fields of spoof SPPs are completely excluded from the metal. In the actual case with finite ε_m, the field penetration into the metal in region III is represented by the second term in the square brackets in Eq. (16), which vanishes in the PEC case. The field penetration into the metal in region II is mainly reflected in the quantity U in Eq. (16), which includes the factors $S_{mn}^{\pm}$. In this case, spoof SPPs on the corrugated wire are lossy due to the absorption in the metal, thus their propagation constants are complex. In our formulation, we have neglected higher-order terms of $1/\sqrt{-\varepsilon_m}$ in Eq. (15), so the dispersion relation (17) is valid for terahertz or lower frequencies, at which $|\varepsilon_m|$ is very large.

To validate the proposed dispersion relation for spoof SPPs on a corrugated metal wire, we first analyze its convergence for modal expansion. In what follows, the metal is assumed to be Al, and its dielectric properties are modeled by a Drude model with the parameters taken from Refs. 16 and 17. Here, as an example, the outer radius is $R=100$ μm and the lattice constant is $d=50$ μm. Two different groove cases are analyzed: (1) $a=0.2d$, $h=d$; (2) $a=0.6d$, $h=0.9d$. For both cases, the asymptotic frequencies, evaluated at $\mathrm{Re}(\beta)=\pi/d$ (i.e., the border of the first Brillouin zone), have the same value of $f_s=1.1$ THz. It should be noted that our method based on Eq. (17) solves the complex propagation constant of spoof SPPs for a given frequency and that the asymptotic frequency for the corrugated wire cannot be calculated directly. The propagation constants at some discrete sample frequencies are first calculated from Eq. (17), then the asymptotic frequency, at which the real part of propagation constant is equal to π/d, is obtained by using Lagrange interpolation polynomial of degree 2. We take a frequency of $f=0.8$ THz for spoof SPPs. The calculated results are plotted in Fig. 1, where the corresponding results obtained within the PEC approximation are included as squares for comparison. As seen from Fig. 1(a), $\mathrm{Re}(\beta)$ converges rapidly, and the results obtained with the single-mode ($m=0$) approximation are accurate within 5% for both cases. The difference between the values of $\mathrm{Re}(\beta)$ for Al and those for PEC are almost negligible, meaning that the model with the PEC approximation is valid for analyzing the dispersion of spoof SPPs (at terahertz frequencies). However, this model does not offer any information on the loss of these SPPs. Figure 1(b) shows the values of $\mathrm{Im}(\beta)$ calculated from Eq. (17). The result within the single-mode approximation is always larger than the accurate value, and its relative error is 2.4% for the case with $a=0.2d$ and nearly 10% for the case with $a=0.6d$. Our analysis indicates that in the latter case, the relative error becomes 21.6% when $f=1.05$ THz. Evidently, a few modes with high orders become important when the groove width is large, especially at frequencies close to the asymptotic frequency. In our numerical calculations throughout this paper, 21 terms (i.e., $n=-10, -9, \ldots, 9, 10$) are employed in the space-harmonics expansion of the fields in regions I and III, which ensures the numerical results to be accurate within 1%.

As the dispersion properties of spoof SPPs at terahertz frequencies on periodically corrugated wires have been well described in Ref. 11, here we focus on studying the loss properties of these spoof SPPs. Figure 2(a) shows the calculated loss for a typical example in Ref. 11, which has the geometric parameters as follows: $R=100$ μm, $d=50$ μm, $a=0.2d$, and $h=d$. As seen in Fig. 2(a), the attenuation coefficient of spoof SPPs on the corrugated Al wire grows rapidly with increasing frequency, and it reaches nearly 1 cm^{-1} when $f=0.8$ THz, which is almost 100 times larger than that of SPPs on a smooth Al wire of radius $R=100$ μm. It is clear physically that the loss of spoof SPPs is larger when the fields are more strongly confined to the wire. Evidently, the field confinement enhances as the frequency increases. This is displayed in Fig. 3, where the distribution of the **H** field in a unit cell of the wire structure is plotted for various frequencies. The fields of the surface wave are almost concentrated in the structured wire when $f=0.8$ and 1 THz.

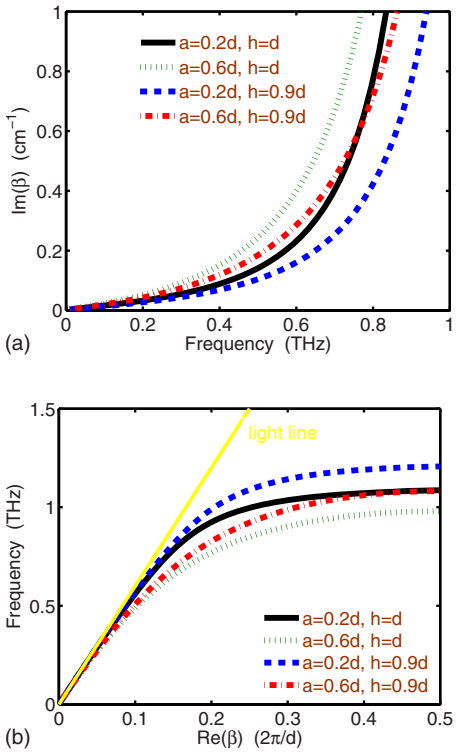

FIG. 2. (Color online) (a) Attenuation coefficients and (b) dispersion relations of spoof SPPs for various groove cases. The lattice constant $d=50$ μm, and $R=100$ μm.

It is interesting to analyze the dependence of the loss of spoof SPPs on the groove parameters. The loss of spoof SPPs for various groove cases is shown in Fig. 2(a). If we change only one parameter of the groove geometry and keep the others unchanged in the calculations, we find the following properties for a given frequency: (1) a larger groove width corresponds to a larger SPP loss; (2) a small reduction of groove depth leads to a significant reduction in the SPP loss. The dispersion curves of spoof SPPs for different groove cases are shown in Fig. 2(b). Evidently, a larger groove width or depth correspond to a lower asymptotic frequency, and the asymptotic frequency is more sensitive to the groove depth, as indicated in Ref. 11. For a given frequency, a lower asymptotic frequency leads to a greater departure of the propagation constant of spoof SPPs from the light line.

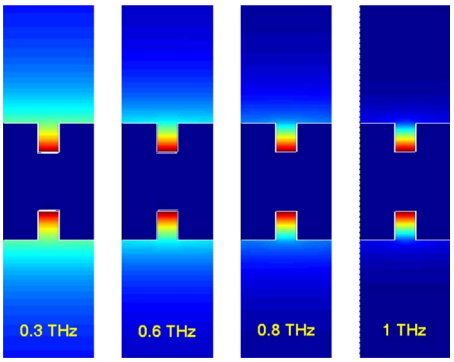

FIG. 3. (Color online) Spatial variation of the amplitude of the **H** field in a unit cell of the wire structure for various frequencies. The wire has the following parameters: $d=50$ μm, $a=0.2d$, $h=d$, and $R=100$ μm.

Correspondingly, the radial component of the wave vector $q_0^{(1)}=\sqrt{\beta^2-k_0^2}$ becomes larger, thus enhancing the field confinement. As a result, the loss of the spoof SPPs increases. However, when two wire structures in comparison have different groove width and depth simultaneously, for example, the case with $a=0.2d$ and $h=d$ and the case with $a=0.6d$ and $h=0.9d$ in Fig. 2 (referred to as the first and second cases, respectively), the situation of spoof SPPs becomes complicated. As shown in Fig. 2(a), the loss of spoof SPPs at lower frequencies in the first case is lower than that in the second case, which is expected because the propagation constant of the spoof SPPs for the first case is less than that for the second case [see Fig. 2(b)]. However, when $f>0.8$ THz, the loss of spoof SPPs in the first case is larger than that in the second case, while the propagation constant of the spoof SPPs in the first case is still less than that in the second case. This is an interesting phenomenon. As seen from Fig. 2(b), the propagation constants of spoof SPPs on these two structures are close to each other and far from the light line when $f>0.8$ THz, therefore their field confinements are almost the same although the confinement in the second case is slightly better than in the first case. In this situation, we have to have a closer examination of the effect of field penetration on the loss of SPPs. Let us consider the major components of the fields in regions I and II, and their matching conditions at the interface $\rho=R$. In the z direction, the major component of the fields in region I varies as $\exp(i\beta z)$, while the fields of the lowest-order groove mode are almost uniform in the groove. As the propagation constant of spoof SPPs is quite large when $f>0.8$ THz, the variation of the fields in region I over the groove width noticeably affects the field excitation inside the groove; thus, the fields of the lowest-order mode are less efficiently excited for the case with $a=0.6d$ than those for the case with $a=0.2d$. Consequently, the weaker penetrated fields in the metal in regions II and III correspond to a smaller energy dissipation, leading to a lower loss for spoof SPPs in the case with $a=0.6d$. Though some higher-order groove modes are also excited, their fields decay rapidly along the groove depth direction, and, consequently, their energy dissipation in the metal is much smaller than that of the lowest-order mode. Importantly, this phenomenon implies that there exists a possibility of optimum design of spoof SPPs to achieve both low propagation loss and good field confinement within a certain frequency range.

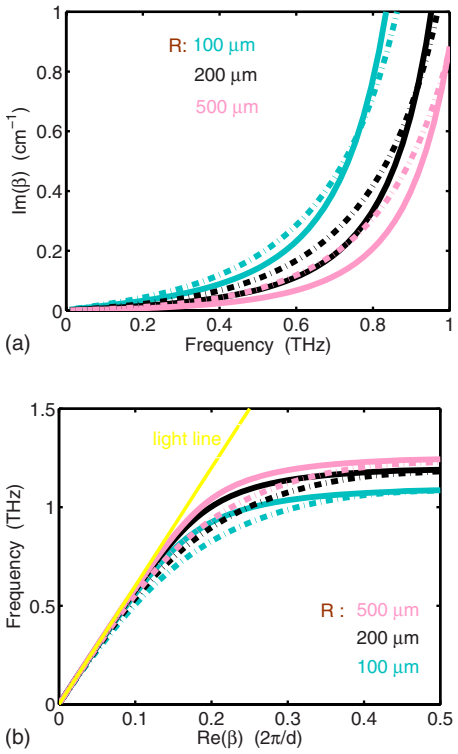

FIG. 4. (Color online) (a) Attenuation coefficients and (b) dispersion relations of spoof SPPs for different outer radii $R=100$, 200, and 500 μm. The solid lines correspond to the groove case of $a=0.2d$ and $h=d$, and the dot-dashed lines correspond to the case of $a=0.6d$ and $h=0.9d$. The lattice constant is $d=50$ μm.

The dependence of the loss of spoof SPPs on the outer radius (R) is also analyzed, and the calculated results are plotted in Fig. 4(a), where two different types of groove geometry are considered: (1) $a=0.2d$ and $h=d$ (solid lines); (2) $a=0.6d$ and $h=0.9d$ (dot-dashed lines). In both cases, for a given frequency, the loss of spoof SPPs decreases as R is increased. In the typical case of $a=0.2d$ and $h=d$, the attenuation coefficient for $f=0.8$ THz is reduced from 1 to 0.2 cm^{-1} when R is increased from 100 to 500 μm. This phenomenon can be easily explained from the dispersive behavior of spoof SPPs shown in Fig. 4(b). So the low-loss propagation of spoof SPPs can be more easily achieved on corrugated wires with larger R.

For spoof SPPs at terahertz frequencies, the most interesting phenomena are their unusual behaviors such as energy concentration and superfocusing, as described in Ref. 11, where the relevant studies are made within the PEC approximation. However, from the above analysis, it seems that the absorption of metal at terahertz frequencies would have severe influence on the performance of these behaviors, as the loss of spoof SPPs is often considerably large when the fields are highly confined to the wire. To check this, we analyze the same example used in Ref. 11 for energy concentration, but here the metal is Al instead of a PEC. The outer radius $R=100$ μm is fixed and the inner one (r) is reduced from

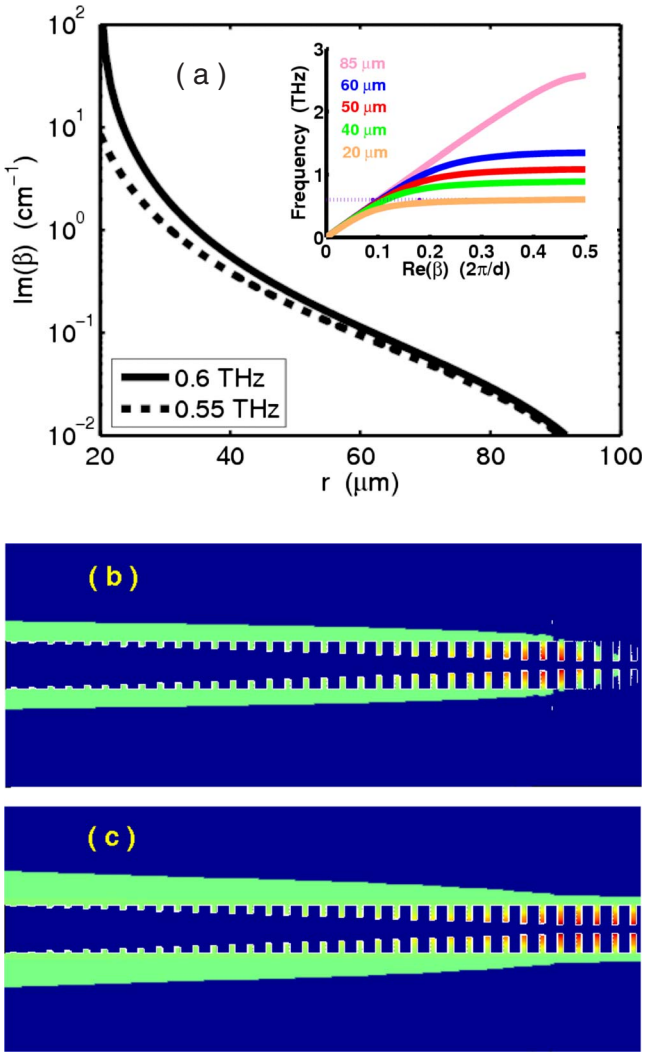

FIG. 5. (Color online) (a) Attenuation coefficient of spoof SPPs versus the inner radius r. The outer radius $R=100$ μm and $d=50$ μm are fixed. The inset shows the dispersion relations for $r=85$, 60, 50, 40, and 20 μm. [(b) and (c)] Field concentration via adiabatic reduction of r in the Al wire for the frequencies $f=0.6$ and 0.55 THz.

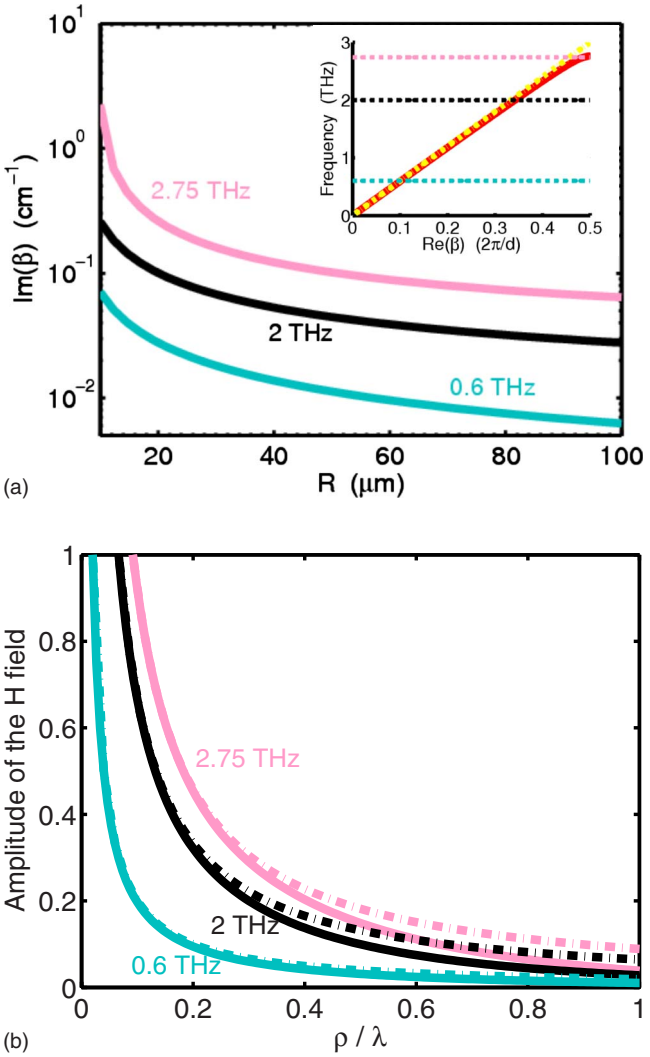

FIG. 6. (Color online) (a) Attenuation coefficient of spoof SPPs versus the outer radius R for three different frequencies $f=0.6$, 2, and 2.75 THz. The groove depth $h=5$ μm and $d=50$ μm are fixed. The inset shows the dispersion relation for $R=10$ μm, where the three frequencies are indicated. (b) Distribution of the amplitude of the **H** field in the radial direction for $R=10$ μm at the frequencies $f=0.6$, 2, and 2.75 THz. The corresponding results for the smooth Al wire with radius $R=10$ μm are plotted as dot-dashed lines for comparison.

95 to 20 μm in steps of 2.5 μm. This special region of decreasing r is followed by a regular region with constant $r=20$ μm. The groove width $a=10$ μm and $d=50$ μm are constants. We take a frequency of $f=0.6$ THz as in Ref. 11. Figure 5(a) shows the attenuation coefficient of spoof SPPs on periodically corrugated wires with various r. The loss of spoof SPPs grows rapidly with decreasing r, and it is up to nearly 10^2 cm^{-1} at $r=20$ μm. Our analysis shows that even if the propagation of the spoof SPPs is adiabatical (without any back reflection and scattering) over the special region, the power loss due to the metal absorption is up to nearly 90%, as illustrated in Fig. 5(b), where the distribution of the **H** field is plotted for the adiabatical propagation. As the frequency (0.6 THz) is very close to the asymptotic frequency for $r=20$ μm, the **H** field is finally concentrated in a region ten times smaller than the wavelength on the surface of the wire, but this energy concentration has no practical meaning due to the severe loss of energy during the concentration process. However, if we take a little smaller frequency of $f=0.55$ THz instead, we find that the power loss for the energy concentration is reduced to 20%, and the **H** field is still concentrated in a region six times smaller than the wavelength, as illustrated in Fig. 5(c).

We finally analyze the superfocusing of terahertz radiation at the tip of a corrugated Al cone. This phenomenon was studied in Ref. 11 within the PEC approximation. The conical structure considered here has the same geometric parameters as in Ref. 11: $d=50$ μm, $a=10$ μm, and $h=5$ μm. In this cone, the outer radius of the Al wire (R) is reduced from 100 to 10 μm over a distance of 2 nm, while the depth of the grooves is constant. To estimate the energy loss of spoof

SPPs during the focusing process, we calculate the attenuation coefficient of spoof SPPs on periodically corrugated wires with various R for three different frequencies $f=0.6$, 2, and 2.75 THz, and the results are plotted in Fig. 6(a). Our analysis indicates that the absorbed power of spoof SPPs for the adiabatical propagation over this cone is only 0.6% for $f=0.6$ THz, and it becomes 2.3% for $f=2$ THz and 6.6% for $f=2.75$ THz, where the last frequency is very close to the asymptotic frequency for $R=10$ μm. So the absorption effect can be neglected for the superfocusing of terahertz radiation. Apparently, the achievement of superfocusing at the tip of this cone mainly relies on the high localization character of the surface mode of the periodically corrugated wire with $R=10$ μm. The distribution of the amplitude of the **H** field of this mode in the radial direction for the frequencies $f=0.6$, 2, and 2.75 THz is plotted in Fig. 6(b). For comparison, the corresponding results for a smooth Al wire of radius $R=10$ μm are included as dot-dashed lines in the figure. The data in Fig. 6(b) are normalized to their values at $\rho=R$. Surprisingly, the SPPs on the smooth thin wire seem to be as highly localized as those in the corrugated thin wire, implying that a smooth metal cone can also exhibit superfocusing of terahertz radiation.

In conclusion, a rigorous method for analyzing spoof SPPs on a periodically corrugated metal wire has been formulated based on a modal expansion of electromagnetic fields. Compared with the previous method, our method is able to calculate the loss of spoof SPPs propagating along the wire, as it takes into account the finite conductivity of the wire. Also, higher-order modes within the wire grooves are included in our method. The convergence analysis shows that a few modes with high orders are not negligible when the groove width is relatively large. In the terahertz frequency range, the properties of the loss of spoof SPPs on corrugated Al wires have been analyzed. The loss of the spoof SPPs grows significantly as the field confinement is enhanced, and the loss is often considerably large when the frequency is close to the asymptotic frequency. However, the subwavelength field confinement is still available with a tolerable loss. The absorption effect on the energy concentration and superfocusing of terahertz radiation has also been analyzed. This effect would impose a limit to the level of the energy concentration, but has negligible influence on the superfocusing.

This work was supported by the Ministry of Education (Singapore) under Grants No. R263000357112 and No. R263000357133.

*elechenx@nus.edu.sg

[1] T. W. Ebbesen, H. J. Lezec, H. F. Ghaemi, T. Thio, and P. A. Wolff, Nature (London) **391**, 667 (1998).
[2] J. B. Pendry, Phys. Rev. Lett. **85**, 3966 (2000).
[3] W. L. Barnes, A. Dereux, and T. W. Ebbesen, Nature (London) **424**, 824 (2003).
[4] C. Girard, Rep. Prog. Phys. **68**, 1883 (2005).
[5] D. Qu, D. Grischkowsky, and W. Zhang, Opt. Lett. **29**, 896 (2004).
[6] H. Cao and A. Nahata, Opt. Express **12**, 1004 (2004).
[7] K. Wang and D. M. Mittleman, Nature (London) **432**, 376 (2004).
[8] J. B. Pendry, L. Martin-Moreno, and F. J. Garcia-Vidal, Science **305**, 847 (2004).
[9] F. J. Garcia-Vidal, L. Martin-Moreno, and J. B. Pendry, J. Opt. A, Pure Appl. Opt. **7**, S97 (2005).
[10] A. P. Hibbins, B. R. Evans, and J. R. Sambles, Science **308**, 670 (2005).
[11] S. A. Maier, S. R. Andrews, L. Martin-Moreno, and F. J. Garcia-Vidal, Phys. Rev. Lett. **97**, 176805 (2006).
[12] Y. Chen, Z. Song, Y. Li, M. Hu, Q. Xing, Z. Zhang, L. Chai, and C. Y. Wang, Opt. Express **14**, 13021 (2006).
[13] K. Wang and D. M. Mittleman, Phys. Rev. Lett. **96**, 157401 (2006).
[14] J. A. Kong, *Electromagnetic Wave Theory* (Cambridge, Massachusetts, 2005).
[15] A. W. Snyder and J. D. Love, *Optical Waveguide Theory* (Chapman and Hall, London, 1983).
[16] D. R. Lide, *CRC Handbook of Chemistry and Physics* (CRC, Boca Raton, FL, 2004).
[17] N. W. Ashcroft and N. D. Mermin, *Solid State Physics* (Saunders College, Philadelphia, 1976).